ACS APPLIED MATERIALS & INTERFACES

Research Article

www.acsami.org

Photoluminescent Graphene Nanoparticles for Cancer Phototherapy and Imaging

Md Nurunnabi,[†] Zehedina Khatun, [‡] Gerald R. Reeck,[∥] Dong Yun Lee,*[,⊥] and Yong-kyu Lee*[,§,‡]

[†]Department of Polymer Science and Engineering, [‡] Department of Green Bioengineering, [§]Department of Chemical and Biological Engineering, Korea National University of Transportation, Chungju, 380-702, Republic of Korea

[∥]Department of Biochemistry, Kansas State University, Manhattan, Kansas 66506, United States

[⊥]BK21 PLUS Future Biopharmaceutical Human Resources Training and Research Team, Institute for Bioengineering and Biopharmaceutical Research, Department of Bioengineering, College of Engineering, Hanyang University, Seoul 133-791, Republic of Korea

Supporting Information

ABSTRACT: Graphene-based nanomaterials are of great interest in a wide range of applications in electronics, the environment, and energy as well as in biomedical and bioengineering. Their unique properties make them generally applicable as prognostic, diagnostic, and therapeutic agents in cancer. In this work, we focused on photodynamic and photothermal therapeutic properties of our previously synthesized carboxylated photoluminescent graphene nanodots (cGdots). The cGdots are ∼5 nm in diameter and excited at 655 nm. Our findings reveal that, upon laser irradiation by near-infrared (wavelength 670 nm) sensitizer, electrons of the cGdots starts to vibrate and form electron clouds, thereby generating sufficient heat (>50 °C) to kill the cancer cells by thermal ablation. The generation of singlet oxygen also occurs due to irradiation, thus acting similarly to pheophorbide-A, a well-known photodynamic therapeutic agent. The cGdots kills MDA-MB231 cancer cells (more than 70%) through both photodynamic and photothermal effects. The cGdots were equally effective in the *in vivo* model of MDA-MB231 xenografted tumor-bearing mice also as observed for 21 days. The cGdot was intravenously injected, and the tumor was irradiated by laser, resulting in final volume of tumor was ∼70% smaller than that of saline-treated tumor. It indicates that the growth rate of cGdot-treated tumor was slower compared to saline-treated tumor. The synthesized cGdots could enable visualization of tumor tissue in mice, thereby illustrating their use as optical imaging agents for detecting cancer noninvasively in deep tissue/organ. Collectively, our findings reveal that multimodal cGdots can be used for phototherapy, through photothermal or photodynamic effects, and for noninvasive optical imaging of deep tissues and tumors simultaneously.

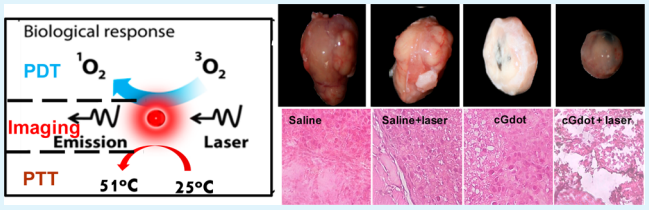

KEYWORDS: *graphene nanodots, noninvasive imaging, phototherapy, biomaterial, in vivo*

1. INTRODUCTION

Multimodal nanoparticles have been studied extensively for improving medical diagnosis and treatment of various diseases.[1,2] Theranostic strategies, using materials that combine diagnostic with therapeutic agent, have the potential to overcome undesirable differences in biodistribution and selectivity that currently exist between distinct imaging and therapeutic agents.[3,4] Several research studies have recently indicated that zero-dimensional (0D) multi/mono layer graphene has been found to be an emerging carrier for drug delivery.[5,6] This includes, for example, use of hybrid SiO_2-coated quantum dot-conjugated graphene, for targeted fluorescent imaging, tracking, and monitoring of drug delivery, as well as cancer photo (photothermal) therapy.[7−11] The most promising aspects of utilizing carboxylated photoluminescent graphene nanodots (cGdots) as theranostic agents is that these nanoparticles have high surface area-to-volume ratios, thus providing high loading capacities. The planar surface of graphene quantum dots is considered an additional window for drug delivery since many drug molecules could be placed on both surfaces (top and bottom) of graphene through physical or chemical interaction.[12] Thus, graphene quantum dots are one of the most attractive materials to propel cancer treatment toward individualized imaging and treatment.

Cancer phototherapy is one of the emerging fields of research for cancer treatment. The concepts of photo/light therapy is based on two unique properties of photosensitizers (a material when exposed to light of specific wavelength) that generate cytotoxic reactive oxygen species (photodynamic) or generate heat (photothermal) that are capable of killing cells through photoablation. Because photosensitizers are typically harmless without light, tumor treatment can be precisely targeted by selective illumination, thus limiting damage to surrounding healthy tissues. In addition, photodynamic therapy

Received: April 15, 2014
Accepted: July 23, 2014
Published: July 23, 2014

has been shown to damage tumor vasculature through direct effects on vascular endothelial cells.[13] However, clinical application of photodynamic therapy is limited due to the hydrophobic nature and poor tumor selectivity of the existing photosensitizers. Recently, extensive efforts have been devoted to design various delivery systems for photosensitizers, including self-assembled nanoparticles and polymer/photosensitizer conjugates. In some studies, the aqueous solubility of the photosensitizers was improved by loading the hydrophobic photosensitizer into the cores of the amphiphilic copolymer or by conjugating with hydrophilic polymers.[14] Photothermal therapy is a new promising form of cancer phototherapy using nontoxic light-sensitive compounds that are exposed selectively to light, whereupon they become toxic, in a very targeted way, to malignancies through generating heat.[15] This approach provides specialized chemotherapeutic treatment for cancer patients either without surgery or synergistically,[16] and it has attracted significant attention in recent years as a promising alternative or supplement to general cancer therapies. Numerous reports have shown encouraging therapeutic effects of photothermal therapy in animal experiments, using various light-absorbing nanomaterials. Ideal photothermal therapeutic agents should exhibit strong absorbance in the near-infrared region, which is a transparency window for biological tissues, allowing efficient conversion of the absorbed near-infrared optical energy into heat. In addition to their tumor-homing ability, the biocompatibility of photothermal therapeutic agents is of significant concern.

A near-infrared optical imaging probe is the best candidate for *in vivo* imaging of deep veins, tissues, and organs in addition to early detection of cancer from bloodstream. Over the past few years, near-infrared quantum dots (Qdots) have been developed and used for deep-tissue imaging, due to their excellent photostability and photoluminescence properties. However, these Qdots are far from approval for clinical trials due to their severe toxicity.[17] Recently, photoluminescent graphene nanoparticles were introduced by several groups as having excitation and emission wavelengths in the range of 400 to 600 nm.[18−21] We have also previously reported on the synthesis of visible to near-infrared photoluminoscent graphene nanoparticles.[22] We have also widely studied the toxicology of Gdots in different cell lines and in rats over a 22 d period of intravenous (IV) administration. No signs and symptoms of severe toxicity were observed after the IV administration of the cGdots, as the results showed a similar profile with the control groups.[23] By controlling the reaction parameters, we produced cGdots excited at 670 nm. When cGdot irradiates by external laser source, it absorbs energy and undergoes a $\pi-\pi^*$ transition. In the case of a conjugated π system, the energy gap for $\pi-\pi^*$ transition is smaller than the isolated unsaturated bond.[24−26] As a result, the conjugated π system become larger, the energy gap for a $\pi-\pi^*$ transition becomes increasingly narrow, and thus the wavelength of light absorbed correspondingly becomes longer. Our cGdots contain extended conjugated π systems and absorb light from visible to near-infrared ranges.[27] On the basis of the chemical structure of cGdots, we assumed that a photodynamic therapeutic effect could be obtained through singlet oxygen generation upon laser irradiation. *In vitro* models were developed to observe photothermal and photodynamic therapeutic effects through thermogenesis and singlet oxygen genesis. These effects were compared to those obtained using a commercial photosensitizer (PheA) or reduced graphene oxide with high near-infrared absorbance.

Our results indicate that the cGdots can be used, without chemical modification, as multimodal probes for simultaneous cancer optical imaging and therapy. The nanosized cGdots with ∼5 nm in diameter are observed to kill ∼70% of cancer cells in both *in vitro* and *in vivo* studies. Thus, tumor growth dramatically inhibits compared to saline-treated model upon laser irradiation of solid tumor by 670 nm laser source. Our findings suggest that cGdot can be considered as an attractive optical contrast agent in biomedical applications for deep-tissue imaging, organ imaging, as well as cancer phototherapy.

2. EXPERIMENTAL SECTION

Materials. Pitch carbon fiber was purchased from Fiber Glast Development Corporation (Carr Drive Brookville, OH). Sulfuric acid, nitric acid, sodium hydroxide, and sodium carbonate were purchased from Sigma-Aldrich (St. Louis, MO). Cell culture reagents, including fetal bovine serum (FBS), Dulbecco's Modified Eagle Medium (DMEM), penicillinestreptomycin, trypsin/ethylenediaminetetraacetic acid, and Dulbecco's phosphate buffer saline (PBS) were purchased from Gibco BRL (Carlsbad, CA, USA). 3-(4,5-dimethylthiazol-2-yl)-2 and 5-diphenyl tetrazolium bromide (MTT) were obtained from Amresco Inc. (Solon, OH, USA).

Synthesis and Characterization of Photoluminescent Graphene Nanoparticles. Synthesis and characterization of cGdots have been reported previously[22,23] and were partially modified in this research. In brief, sulfuric acid (40 mL) was added in a beaker. Carbon fiber (100 g) was added to the solvent and sonicated by Ultra sonicator for 10 min. Nitric acid (20 mL) and sulfuric acid (450 mL) were added in a three-neck flask and placed in a heating mantle. Temperature was adjusted to 95 ± 5 °C. The previously sonicated carbon fiber solution was slowly injected into the flask with a syringe injector. The reaction was carried out for 12 h at the same temperature. Excess amount of water (200 mL) was added to the beaker slowly. Sodium hydroxide and sodium carbonate were added to the solution to make the pH 8. The flask was placed in an ice bath, which was temperature-controlled to 0−4 °C with slow stirring. Precipitation was removed from the flask by decantation. Citric acid was added with the solution and stirred for 2 h at room temperature. The graphene Qdots-containing solution were freeze-dried for 48 h, and the powder was obtained.

Raman spectra were recorded with a RenishawIn Via Raman microscope using a 50 objective lens at room temperature, with a 514.5 nm laser beam and 1,800 lines per mm grating. Photoluminescent, excitation, and emission were measured by luminescent analyzer FluoroMate FS-2 (Scinco, Korea). The X-ray diffraction (XRD) data were collected on a Rigaku D/Max Ultima II powder X-ray diffractometer. X-ray photoelectron spectroscopy (XPS) analyses were carried out on a PHI Quantera X-ray photoelectron spectrometer with a chamber pressure of 5×10^{-9} Torr and an Al cathode as the X-ray source. The source power was set at 100 W, and pass energies of 140.00 eV for survey scans and 26.00 eV for high-resolution scans were used. Band-gap values of near-infrared graphene nanoprticles were measured based on the absorbance and reflectance of the respective graphene nanoprticles. The calculation methods have been elaborately discussed elsewhere.[22]

Measurement of Singlet Oxygen Generation. The generation of singlet oxygen was measured by the decrease of fluorescence intensity of 9,10-dimethylanthracene (DMA) utilizing fluorescent spectroscopy as described previously.[14] In brief, a cGdots solution containing 1.184×10^{-2} mM DMA was irradiated at a light intensity of 0.3 W/cm^2 using a 670 nm laser source (LWRL-100 K, Laserwave, China). The decrease in fluorescence intensity of DMA (emission: 380−550 nm, with excitation at 360 nm) as a result of singlet oxygen generation was monitored using a spectrofluorophotometer.

***In Vitro* Photothermal Treatments.** The MDA-MB231 cells were seeded into an eight-well plate with 200 μL of culture medium. To visually observe the photothermal therapeutic efficacy of cGdots, the existing medium was replaced by the medium with cGdots

Scheme 1. Schematic Representative Chemical Structure of near-Infrared cGdots (Excitation Wavelength: 655 nm) for Optical Imaging and Therapy[a]

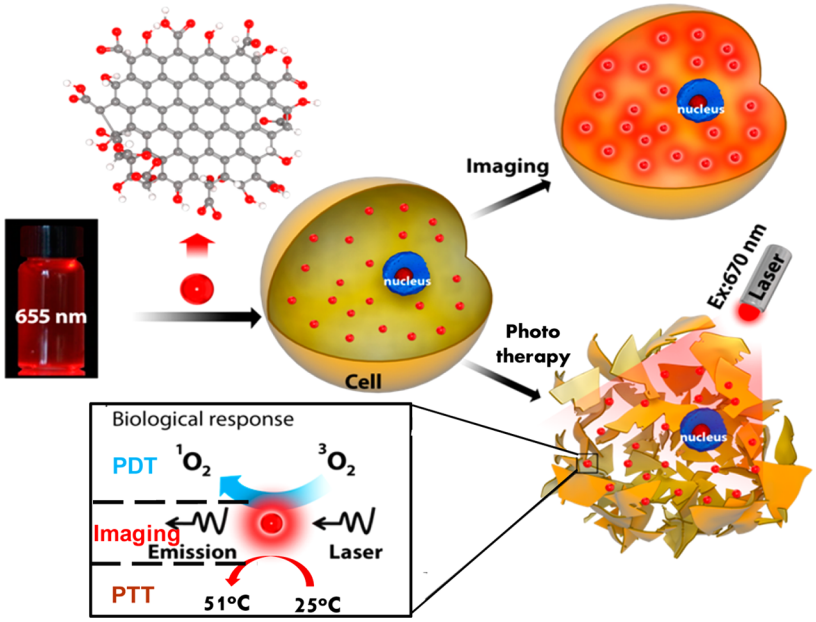

[a]The suspected scheme of cGdots shows presence of carboxyl acid and hydroxyl functional groups located on the edges. It indicates the rapid generation of singlet oxygen as a function of the time of laser exposure, as soon as near-infrared cGdots was uptaken in the cancer cells. Photothermal effect of cGdots could also be observed even if the nanoparticle locates outside the cells. Cellular uptakes of cGdots were easily monitored in real time by confocal laser scanning microscopy. It suggests that the cGdots with ideal size are accumulated within the tumor micro environment by EPR effect.

containing 0.5 mg/mL, and the medium without cGdots was used as the control. The experimental process is reported elsewhere.[28] After 1 h of incubation, the plate was placed in a dark clean bench and irradiated by laser (670 nm, 0.3 W/cm^2) for 30 min. After additional 2 h of incubation, cells were washed with PBS. The cells were stained with calcein-AM (Invitrogen) and incubated for 20 min to visually observe the live cells by confocal laser scanning microscope (CLSM).

Photocytotoxicity Evaluation. *In vitro* phototoxicity study of near-infrared cGdots was examined in MDA-MB231 cell for 24 h of incubation. At 37 °C and 5% CO_2 containing humidified atmosphere, cells were grown in a medium containing MEM with 10% fetal calf serum. After 24 h, the complete medium was suctioned, and cGdots was added into the well at different concentrations (50, 100, 250, and 500 μg/mL) with complete medium. The entire cell containing wells were irradiated by laser (670 nm, 0.3 W/cm^2) for 30 min. After 4 h, 100 μL of MTT solubilizing solution was added and gently shaken for 15 min. Finally, the absorbance of MTT colorimetric assay was measured by Varioskan flash (Thermo Scientific, USA) at a wavelength of 570 nm. The viable quantity of cells was calculated by the following equation:

$$\text{cell viability}(\%) = (\text{absorbance of sample cells} / \text{absorbance of control cells}) \times 100$$

Lactate Dehydrogenase Release Assay. cGdots samples were introduced separately to the cells with different concentrations (50, 100, 250, and 500 μg/mL) and incubated for another 24 h, and the entire cell-containing well was irradiated by laser (670 nm, 0.3 W/cm^2) for 30 min. The positive control was prepared by adding 10 μL of lysis solution to the control cells at 45 min prior to the centrifugation. Then, the centrifugation (1200 rpm × 5 min) was performed. The lactic dehydrogenase (LDH) leakage (% of positive control) is expressed as the percentage of (test − blank)/(positive − blank), where test is the cells exposed to cGdots, positive is the optical density of the positive control cells, and blank is the optical density of the wells without MDA-MB231 cells.

***In Vitro* Cellular Uptake.** For a cellular uptake study of cGdots nanoparticle, the nanoparticles were incubated with the MDA-MB231 cell line. Different concentrations of the cGdots nanoparticles were added to the eight-well plate and incubated for 1 h before observation using a confocal laser scanning microscope. The wells were washed five times by PBS to remove the free particles from the outside of the cell membrane. The cellular images were observed by confocal laser scanning microscope (CLSM) at an excitation filter of 654 nm.

Flow Cytometric Analysis of Apoptosis and Necrosis. The MDA-MB231 cells were cocultured with/without cGdots, incubated for 1 h, and irradiated by laser (670 nm, 0.3 W/cm^2) for 30 min. Flow cytometric analysis was performed on a FACSCalibur flow cytometer (BD Biosciences, Heidelberg, Germany), using a CellQuest Pro software for acquisition and analysis.[29] The size and granularity of cells were assessed using forward scatter (FSC) and side scatter (SSC) analysis, respectively. Necrotic and/or apoptotic cell death was analyzed by double staining with Annexin V-fluorescein isothiocyanate (FITC) and propidium iodide, in which the former binds to early apoptotic cells with exposed phosphatidylserine, while the latter labels the late apoptotic/necrotic cells with membrane damage. Staining was performed according to the instructions by the manufacturer (BD Pharmingen, San Diego, CA).

***In Vivo* Imaging and Biodistribution Analysis.** Molecular imaging was conducted according to our previously published article.[30] In brief, for *in vivo* imaging studies, SKH1 mice were administered 2.5 mg/kg of cGdots through the tail vein. Mice were anesthetized with ketamine (87 mg/kg, Virbac Laboratories, France) and xylazine (13 mg/kg, Kepro B.V., Netherland) via intraperitoneal injection. *In vivo* mice images were taken by a time-domain diffuse optical tomography system. In Experimental Section, mice were placed on the imaging platform. Images were taken at 4 h of post injection. The *ex vivo* images of organs were taken after dissection of the mice. The organs were isolated after 4 h of observation.

Temperature Measurement during Laser Irradiation. The cGdots were dissolved in PBS (2 mg/mL) and dispersed uniformly. MDA-MB231 tumor-bearing nude mice were injected with intratumoral 50 μL of CGdot suspension. PBS (50 μL) was also injected to

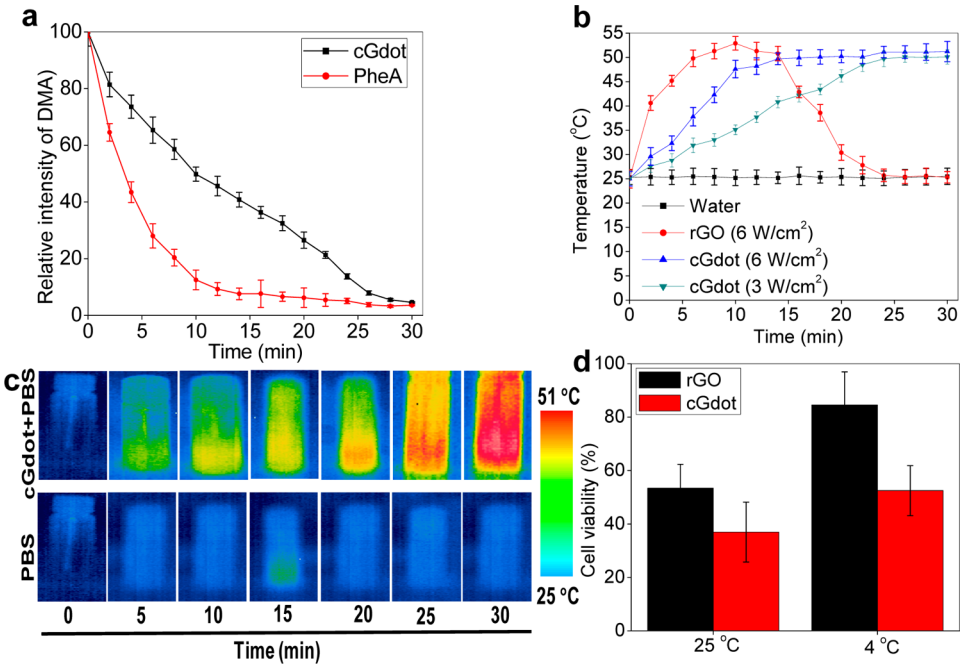

Figure 1. Physicochemical properties of cGdots. (a) Generation of singlet oxygen (DMA) profile of Phephorbide A and cGdots and (b) increment of temperature according to different exposure time of laser irradiation. Data were expressed as mean ± SEM (n = 3). (c) Thermal image of vials containing cGdots according to different exposure time under laser. (d) Cell viability assay of MDA-MB231 cell at 4 and 25 °C, coincubation of rGO, and cGdot for 24 h. Data were expressed as mean ± SEM (n = 6).

the control mice. Both the tumor and vials containing cGdots solution were irradiated by a light intensity of 0.3 W/cm^2 using a 670 nm laser source (LWRL-100 K, Laserwave, China) for up to 30 min. The images were taken by thermal imaging analyzing camera (TH9100MV/WV, NEC san-ei (Japan)) with time intervals (0, 5, 10, 15, 20, 25, and 30 min).

Animals and Tumor Model. Female BALB/c nude mice with an average body weight of 30 g (4−5 weeks old) were purchased from Oriental Bio (Daejeon, South Korea). MDA-MB231 cells (1×10^6) suspended in PBS were administered by subcutaneous injection into the flank region of the nude mice. Tumor volume was calculated as follows: volume = $\pi/6 \times$ length (mm) $\times$ width (mm) $\times$ height (mm).

***In Vivo* Antitumor Study.** The MDA-MB231 tumor-bearing mice were divided into four respective groups, namely, saline, saline with laser, cGdots, and cGdots with laser, which were injected with intratumoral 50 μL of PBS or cGdots containing PBS dispersion (1.5 mg/mL). Each group contained four mice. Tumors of (saline with laser and cGdots with laser) various groups were irradiated by 670 nm laser at 0.3 W/cm^2 for 30 min after every 1 d interval. The tumor volumes and changes in body weight of each mouse were measured. Histology studies of treated tumor tissue were further studied by H&E staining to observe the effect of photothermal therapy *in vivo* after 21 d of observation.

3. RESULTS AND DISCUSSION

Synthesis and Characterization of Photoluminescent Graphene Nanoparticles. The synthesis and characterization method of cGdots has been elaborately described in our previously published articles.[22,23] The method in brief, exfoliation of CF, occurred during sonication and ultrasonication in acidic media (mixture of sulfuric acid and nitric acid). Because of sonication in acids, multilayer and/or monolayered graphene were formed. The remaining multilayered graphene re-exfoliated during reaction for 12 h at 95 ± 5 °C and formed monolayered graphene. These conditions facilitate the formation of a zigzag-shaped nanosize graphene, showing an almost transparent gray-black color solution. The hexagonal nanosized graphene particles formed due to long time exposure in strong acid solution and vigorous stirring. Water was slowly added to the flask after completing the reaction period, and the color of the reaction mixture changed to reddish from brown. Sodium hydroxide (NaOH) was then slowly added to the beaker until the pH reached about 1. Sodium carbonate (Na_2CO_3) was added to adjust the pH to 8. The flask was placed in an ice bath to regulate temperature to 0−4 °C. Precipitation appeared due to slowly stirring at that temperature. The precipitation was removed by decantation, and the photoluminescent cGdots containing the liquid portion was freeze-dried for 48 h. The entire process was performed to protect from photobleaching.

We believed that cGdots could show bimodality for the dual purposes of optical imaging and photodynamic therapy (Scheme 1). A photothermal therapeutic effect of graphene has been previously shown.[31,32] However, to the best of our knowledge, cancer phototherapy and simultaneous imaging has not yet been demonstrated. Previously, we designed cGdots with promising photoluminescence activity.[22,23] The chemical structure of those cGdots was investigated using X-ray photoelectron spectroscopy as well as excitation and emission profiling. We also found that cGdots were zigzag in shape and had a hexagonal structure, containing a number of carboxyl and hydroxyl groups on their edges including numerous unsaturated bonds. These unsaturated bonds resulted in the photosensitization of the cGdots (Supporting Information, Figure S1a). In addition, the cGdots structure was partially folded with arm-chair shape due to interaction among functional groups (Supporting Information, Figure S1b−d), whereas graphene itself has a planar sheet structure.[33] XPS of the cGdots with a high-resolution spectrum of each element demonstrated that the cGdots were mainly composed of carbon (62.4%) and oxygen (35.5%) (Supporting Information, Figure S2 and Table S1). Compared to carbon fiber, we observed (Supporting

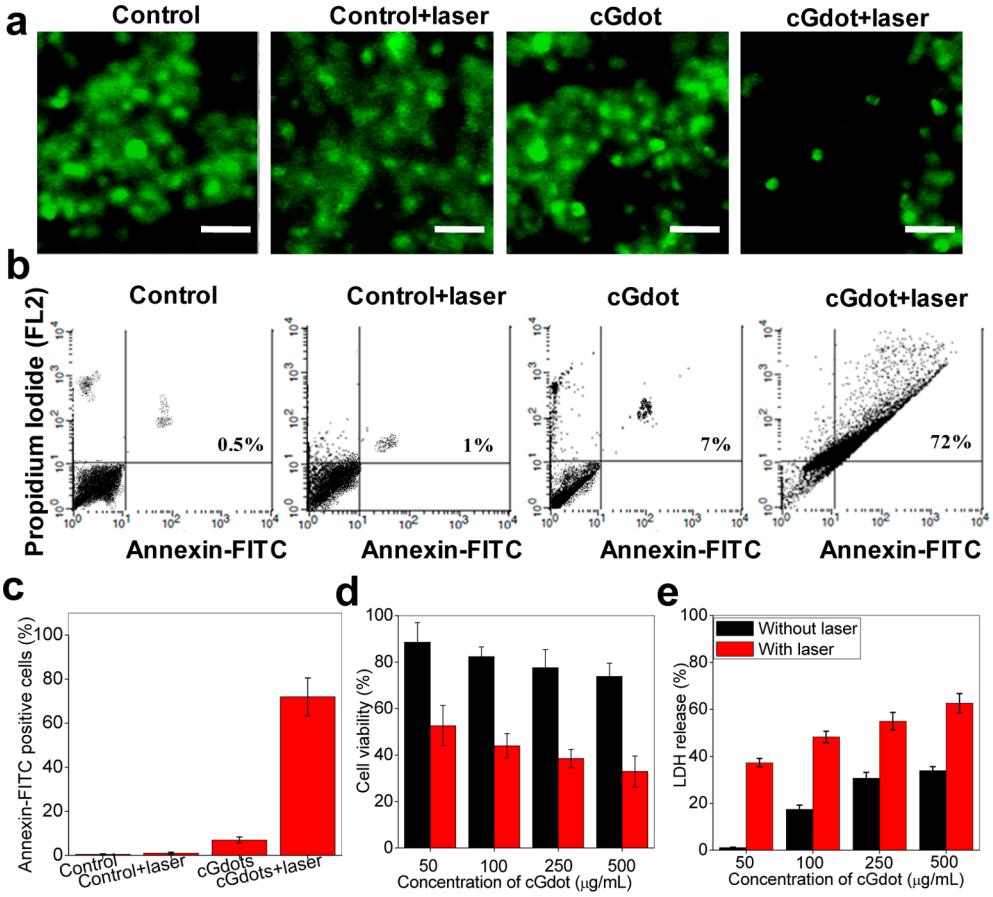

Figure 2. Viability and apoptosis of MDA-MB231 breast cancer cells after the treatment of cGdots with laser irradiation for 30 min. (a) Fluorescence images of MDA-MB231 cells stained by Calcein-AM. Scale bar: 100 μm. (b, c). Flow cytometry analysis of Annexin V-FITC-labeled MDA-MB231 cells for analysis of cellular apoptosis. (d) Viability of MDA-MB231 cells by using MTT assay kit. (e) Cellular toxicity of MDA-MB231 cells by using LDH assay kit. Data were expressed as mean ± SEM (n = 5).

Information, Figure S3) a different Raman shift in our cGdots. The presence of carboxyl and hydroxyl groups in the cGdots was confirmed by FT-IR spectroscopy and ^{1}H NMR spectrometry (Supporting Information, Figure S4).

The cGdots were slowly degraded above 100 °C and showed a glass transition temperature (T_g) of 410 °C (Supporting Information, Figure S5). Using XRD, we found that the peak of crystalline formation of cGdots appeared at 12°, whereas the peaks of carbon fiber and graphene were shown at 25° and 20°, respectively (Supporting Information, Figure S6). Two-dimensional Fourier transform electron imaging showed the hexagonal shape of cGdots. The uniform size and lack of aggregation of the cGdots were confirmed by transmission electron microscopy and dynamic light scattering (Supporting Information, Figure S7).

Photodynamic and Photothermal Properties of cGdots. The (triatomic) ozone molecules absorb radiation energy from an external source and are converted to diatomic molecular oxygen along with a free oxygen atom, also known as free-radical oxygen (Supporting Information, Figure S8). This cGdots with a high level of unsaturation absorbed visible light (wavelength 670 nm) from the external laser irradiation and transferred the energy to surrounding oxygen molecules and unsaturated bonds, resulting in the generation of reactive oxygen species (ROS) such as singlet oxygen and free radicals. Around 85% quenching occurred with 25 min of irradition. Thus, cancer cells can be killed by the cGdots through laser irradiation. The singlet-oxygen quantum yield of the cGdots was determined using 9,10-dimethylanthracene as the singlet oxygen trap (Figure 1a). PheA was used as a control in the singlet-oxygen generation study. Thermogenesis by cGdots was measured upon laser irradiation. During laser irradiation at 670 nm, the temperature change was measured with a photothermal imaging analyzer and laser thermometer. The temperature increased to 50 °C after 30 min of laser irradiation (Figure 1b), confirming the appropriateness of our cGdots for photothermal therapy of cancer. Figure 1c represents the visual thermal images of water and cDots upon time of irradiation. The results described in Figure 1 demonstrated that the cGdots generates reactive singlet oxygen and heat simultaneously upon irradiation. The proposed model shows that the ground-state electrons of cGdots become excited when cGdots absorbs energy from the external laser source, creating electron clouds (Supporting Information, Figure S9). The accelerated electrons generate heat that is fatal to surrounding cells. To more specifically prove that the cell-destruction is either from the photothermal or photodynamic effects of cGdot, another comparative study was conducted. Reduced graphene oxide (rGO) is a well-proven photothermal agent, and cGdots were incubated with cell lines and irradiated at 25 and 4 °C temperature. A noticeable amount (46.5%) of cellular death was observed when rGO-treated cells were irradiated at 25 °C. However, a much higher (63%) amount of cell death was counted in case of cGdot at same condition. On the other hand,

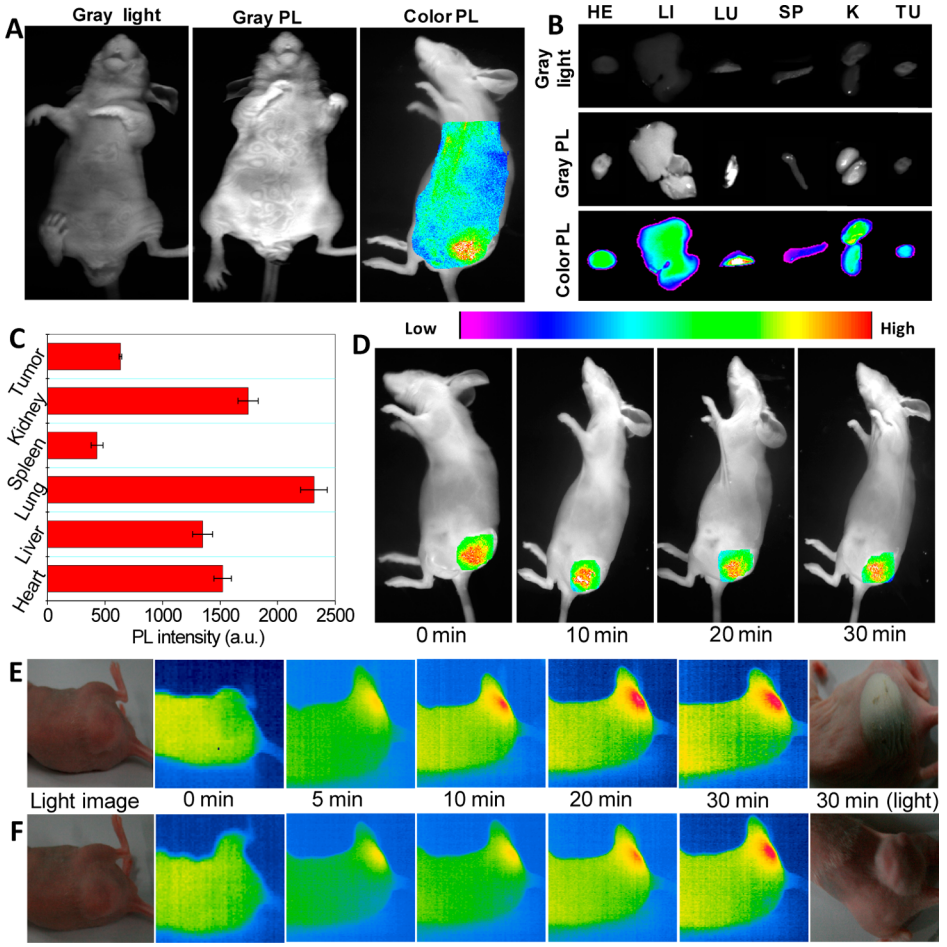

Figure 3. *In vitro* and *in vivo* optical imaging of MDA-MB231 breast cancer cell-bearing mice after injection of cGdots. (a) Non-invasive images of cGdots-treated mice having MDA-MB231 cells *in vivo*. (b) *Ex vivo* images of each harvested organ from cGdots-treated mice having MDA-MB231 cells. HE: heart, LI: liver, LU: lung, SP: spleen, K: kidney, and Tumor: MDA-MB231 cells. (c) Fluorescence intensity of each harvested organ measured by PL analyzer. Data were expressed as mean ± SEM (n = 4). (d) *In vivo* photoquenching profile of cGdots upon laser irradiation up to 30 min through intratumoral injection of cGdots. (e, f) Light dose effect on skin was investigated at 0.6 and 0.3 W/cm^2.

very low amount (15.4%) of cell deaths were counted for rGO when irradiated at 4 °C, but a higher number (47.5%) of cell deaths was observed for cGdot at 4 °C. The results demonstrated that the cGdot generated singlet oxygen at both 25 and 4 °C, but thermogenesis from rGO only occurs at 25 °C. This *in vitro* study provides strong supporting evidence that the cGdot kills cells through both photodynamic and photothermal therapy (Figure 1d).

***In Vitro* Photocancer Therapy in MDA-MB231 Cell Line.** After incubation of cGdots (at 100 μg/mL) with MDA-MB231 cancer cells for 2 h, fluorescence images of the cells were observed using confocal laser scanning microscopy to know the cellular accumulation profile of cGdots (Supporting Information, Figure S13a). The cGdots were internalized and preferentially located in the nuclei (red fluorescence). To confirm the internalization of cGdots, we created three-dimensional histogram images of the cells (Supporting Information, Figure S13b,c). The results demonstrated that the cGdots were internalized through nonspecific binding affinity or the reticuloendothelial system.

The photodestruction capabilities of cGdots were first observed by confocal laser microscopy in cancer cells with lower concentrations such as 50, 100, 250, and 500 μg/mL, though high concentration (2 mg/mL) of Gdot was used during *in vitro* thermogenesis study. For *in vitro* studies, choosing lower concentration is more rational than choosing high concentration, since high concentration of even less-effective materials can show high cellular toxicity and cellular uptake. Therefore, to evaluate the optimum therapeutic concentration, a range of lower concentrations of cGdot suspension were taken into account during *in vitro* toxicity studies instead of high concnetration (2 mg/mL or more). After incubation with the cGdots with MDA-MB231 breast cancer cells, the cells were irradiated for 1 h with an external laser source. Cellular damage was only observed in the cotreatments of cGdots and laser irradiation (Supporting Information, Figure S10). In addition, concentration and laser exposure dependent cytotoxicity of cGdots in MDA-MB231 cells were studied, and the results showed that the cell viability is inversely proportional and cell death is directly proportional to concentration and laser exposure duration. (Supporting Information, Figures S11 and S12). After cotreatment of cGdots and laser irradiation, the viable MDA-MB231 cells were were stained with Calcein-AM (green fluorescence dye) by incubating for 20 min (Figure 2a). The visible live cells were observed by light microscope and showed less cell viability in cGdots and laser irradiation group compared to that of PBS and laser group. However, cGdots without laser also shows around

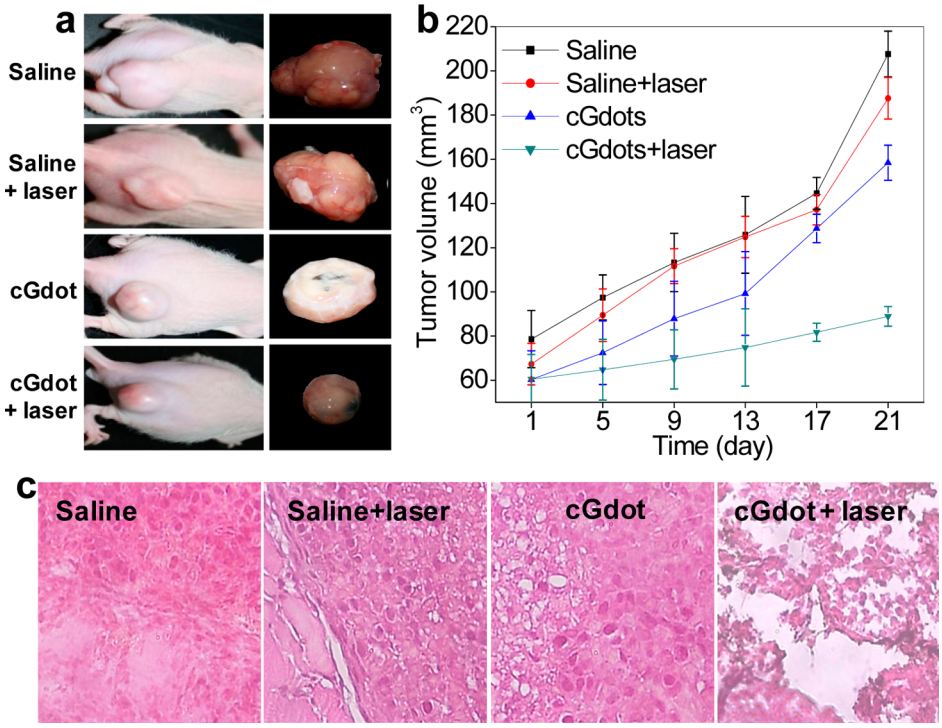

Figure 4. *In vivo* photothermal therapy of MDA-MB231 breast cancer cell-bearing mice after injection cGdots and laser exposure. (a) Morphology of MDA-MB231 cells in subcutaneous space at 21 d after cGdots injection and laser exposure. (b) Plot of tumor size volume in mice. Data were expressed as mean ± SEM (n = 4). (c) Histological analysis of tumor tissue at day 21 after cGdots injection and laser exposure. Magnification: × 400.

90% or more cell viability. Treatment of cGdots with laser irradiation initiated apoptosis, which was confirmed by flow cytometry analysis with Annexin V-FITC labeling (Figure 2b,c). The flow cytometry analysis demonstrated the apoptosis state of the cGdots with laser-treated cells is 72% compared to that of control cells treated by PBS. The laser-irradiation dose-dependence of cell death was again confirmed (Figure 2d,e) with greater than 70% of the cells killed.

***In Vivo* Photocancer Therapy and Real-Time Imaging.** The cGdots were also administered to tumor-bearing mice for *in vivo* imaging and photocancer therapy. For *in vivo* optical imaging studies, nude mice were inoculated with MDA-MB231 breast cancer cells. We then evaluated the optical imaging of cGdots after intravenous injection of cGdots via tail vein using the Kodak Molecular Imaging System as described previously.[34,35] After injection (4 h) of cGdots (2.5 mg/kg), they were broadly (and nonspecifically) distributed in the body including tumor tissue (Figure 3a). The fluorescence intensities of harvested organs were observed (Figure 3b,c), and the cGdots were found to be mostly in the liver, lung, and kidneys. The cGdots were also present at a relatively high level in the MDA-MB231 cell xenografted tumor tissue.

In vivo photobleaching was observed after injection of cGdots into the MDA-MB231 tumor. Optical images were captured at 10, 20, and 30 min of laser irradiation to observe photobleaching profile of cGdots. The photoluminescence intensity of the cGdots slowly decreased over the duration of irradiation because cGdots absorb energy from the laser source (Figure 3d). A laser-energy dose-dependent thermogenesis profile of cGdots in tumor-bearing mice was obtained at 30 min at 0.3 and 0.6 W/cm^2. The results demonstrate that the higher dose of laser energy accelerates thermogenesis (Figure 3e). However, the higher dose (0.6 W/cm^2) is not an optimum dose in terms of skin damage. The skin of the mice was burnt at the higher dose, whereas the damage was not observed in mice with lower dose irradiation (Figure 3f). Therefore, we suggest that irradiation at the lower dose for a longer time is safer than that of higher dose at shorter time to protect the skin as well as surrounding organs.

Finally, the photocancer therapy of cGdots was evaluated in MDA-MB231 tumor-bearing mice to obtain further proof-of-concept of anticancer effect of cGdots. Fifty microliter (2.5 mg/kg dose) of cGdots suspension (1.5 mg/mL in PBS) was injected in 1 d intervals into MDA-MB231 tumor tissue by direct intratumoral injection. Then the tumor tissue was irradiated by laser for 30 min. The results demonstrated that the volume of the MDA-MB231 tumor tissue in mice was not affected when treated with saline, saline with laser, or cGdots alone (Figure 4a,b). However, cGdots injection coupled with laser irradiation significantly inhibited tumor growth (the final size was about one-third that of the controls). The tumor weight from the mice treated with cGdots injection and laser irradiation was also significantly lower compared to the controls (Supporting Information, Figure S14). In our previous study, we observed *in vivo* toxicology of graphene for 21 d with 2.5 and 5 mg/kg dosage. No significant toxicity was observed even in biochemistry studies.[23] Therefore, it is undoubtedly safe and effective to use 2.5 mg/kg in terms of therapeutic aspects as observed from the *in vivo* antitumor study.

Histology of Tumor Tissue. The tumor tissue was examined histologically to evaluate the photothermal and photodynamic therapy obtained by cGdots injection and laser irradiation. As shown in Figure 4c, tumor cells treated with cGdots injection and laser irradiation were strongly damaged. Also cGdots injection along with laser irradiation produced cellular toxicity in and around the tumor tissue (Supporting Information, Figure S15). The cellular damage by cGdots injection and laser irradiation quantified histolocially showed

~70% necrotic cells, whereas no necrotic cells were observed in saline-treated tumors (Supporting Information, Figure S16). cGdots injection and laser irradiation did not produce significant change in body weight compared to control groups (Supporting Information, Figure S17), suggesting that these treatments were nontoxic or at least only slightly toxic.

4. CONCLUSION

This study concluded that these findings demonstrate that photoluminescent cGdots can be used as an optical contrast agent for biomedical imaging and theranostic agent as well, simultaneously. The most imporant and emerging finding from this study is that cGdots is also effective as a photodynamic therapeutic agent when exposed to laser irradiation. Both *in vitro* and *in vivo* investigations provide adequate evidence for proving its feasibility as an active agent to be used for cancer phototherapy and noninvasive biomedical imaging. This study shows cGdot is active for only inhibition of tumor growth, which reduces tumor size by 70% compared to control group. However, further studies are designed to develop more fascinating formulation to destroy the solid tumor through photochemotherapy. We also aim to do further advanced work for observing effects on cellular and molecular levels.

■ ASSOCIATED CONTENT

Supporting Information

Detailed characterization spectra such as FT-IR, XPS, TGA, XRD, and Raman and computer-simulated model of cGdots. This file also contains *in vitro* cellular uptake and toxicity and *in vivo* tumor necrosis and histology data. This material is available free of charge via the Internet at http://pubs.acs.org.

■ AUTHOR INFORMATION

Corresponding Authors

*E-mail: leeyk@ut.ac.kr. Phone: +82-043-841-5224. Fax: +82-043-841-5220. (Y.-k.L)

*E-mail: dongyunlee@hanyang.ac.kr. (D.Y.L.)

Author Contributions

The manuscript was written through contributions of all authors. All authors have given approval to the final version of the manuscript.

Notes

The authors declare no competing financial interest.

■ ACKNOWLEDGMENTS

This research was supported by a Grant (NRF-2010-0021427, NRF-2012R1A2A1A01012042) through the National Research Foundation of Korea (NRF) funded by the Ministry of Education, Science and Technology. We thank Prof. A. Khademhosseini (Harvard-MIT Division of Health Sciences and Technology, Wyss Institute for Biologically Inspired Engineering) for his thoughtful comments and helpful corrections.

■ REFERENCES

(1) Weissleder, R.; Pittet, M. J. Imaging in the Era of Molecular Oncology. *Nature* **2008**, *452*, 580−589.

(2) Sanz, J.; Fayad, Z. A. Imaging of Atherosclerotic Cardiovascular Disease. *Nature* **2008**, *451*, 953−957.

(3) Wang, Y.; Brown, P.; Xia, Y. Nanomedicine: Swarming Towards the Target. *Nat. Mater.* **2011**, *10*, 482−483.

(4) Seo, W. S.; Lee, J. H.; Sun, X.; Suzuki, Y.; Mann, D.; Liu, Z.; Terashima, M.; Yang, P.; McConnell, C. M. V.; Nishimura, D. G.; Dai, H. FeCo/Graphitic-Shell Nanocrystals as Advanced Magnetic-Resonance-Imaging and Near-Infrared Agents. *Nat. Mater.* **2006**, *5*, 971−976.

(5) Charlotte, A. E. H.; Shuguang, Z. Nanotechnology: Peptides as Biological Semiconductors. *Nature* **2010**, *468*, 516−517.

(6) Gao, X.; Gao, X.; Cui, Y.; Levenson, R. M.; Chung, L. W.; Nie, S. *In Vivo* Cancer Targeting and Imaging with Semiconductor Quantum Dots. *Nat. Biotechnol.* **2004**, *22*, 969−976.

(7) Dupont, K. M.; Sharma, K.; Stevens, H. Y.; Boerckel, J. D.; García, A. J.; Guldberg, R. E. Human Stem Cell Delivery for Treatment of Large Segmental Bone Defects. *Proc. Natl. Acad. Sci. U.S.A.* **2010**, *107*, 3305−3310.

(8) Chan, W. C. W.; Nie, S. Quantum Dot Bioconjugates for Ultrasensitive Nonisotopic Detection. *Science* **1998**, *281*, 2016−2018.

(9) Li, J.; Zhao, M. X.; Su, H.; Wang, Y. Y.; Tan, C. P.; Ji, L. N.; Mao, Z. W. Multifunctional Quantum-Dot-Based Sirna Delivery for HPV18 E6 Gene Silence and Intracellular Imaging. *Biomaterials* **2011**, *32*, 7978−87.

(10) Nie, S.; Emory, S. R. Probing Single Molecules and Single Nanoparticles by Surface-Enhanced Raman Scattering. *Science* **1997**, *275*, 1102−1106.

(11) Knipe, J. M.; Peters, J. T.; Peppas, N. A. Theranostic Agents for Intracellular Gene Delivery with Spatiotemporal Imaging. *Nano Today* **2013**, *8*, 21−38.

(12) Chen, X.; Zhou, X.; Han, T.; Wu, J.; Zhang, J.; Guo, S. Stabilization and Induction of Oligonucleotides I-Motif Structure via Graphene Quantum Dots. *ACS Nano* **2013**, *7*, 531−537.

(13) Zhang, Y.; Aslan, K.; Previte, M. J. R.; Geddes, C. D. Plasmonic Engineering of Singlet Oxygen Generation. *Proc. Natl. Acad. Sci. U.S.A.* **2008**, *105*, 1798−1802.

(14) Li, L.; Nurunnabi, M.; Nafiujjaman, M.; Lee, Y.; Huh, K. M. GSH-Mediated Photoactivity of Pheophorbide A-Conjugated Heparin/Gold Nanoparticle for Photodynamic Therapy. *J. Controlled Release* **2013**, *171*, 241−250.

(15) You, J.-O.; Guo, P.; Auguste, D. T. A Drug-Delivery Vehicle Combining the Targeting Aand Thermal Ablation of HER2+ Breast-Cancer Cells with Triggered Drug Release. *Angew. Chem., Int. Ed.* **2013**, *52*, 1−7.

(16) Datta, S. N.; Allman, R.; Loh, C.; Mason, M.; Matthews, P. N. Effect of Photodynamic Therapy in Combination with Mitomycin C on A Mitomycin-Resistant Bladder Cancer Cell Line. *Br. J. Cancer* **1997**, *76*, 312−317.

(17) Ye, L.; Yong, K. T.; Liu, L.; Roy, I.; Hu, R.; Zhu, J.; Cai, H.; Law, W. C.; Liu, J.; Wang, K. A Pilot Study in Non-Human Primates Shows No Adverse Response to Intravenous Injection of Quantum Dots. *Nat. Nanotechnol.* **2012**, *7*, 453−458.

(18) Yan, X.; Cui, X.; Li, L. S. Synthesis of Large, Stable Colloidal Graphene Quantum Dots with Tunable Size. *J. Am. Chem. Soc.* **2010**, *132*, 5944−5945.

(19) Cheng, H.; Zhao, Y.; Fan, Y.; Xie, X.; Qu, L.; Shi, G. Graphene-Quantum-Dot Assembled Nanotubes: A New Platform for Efficient Raman Enhancement. *ACS Nano* **2012**, *6*, 2237−2242.

(20) Son, D. I.; Kwon, B. W.; Park, D. H.; Seo, W. S.; Yi, Y.; Angadi, B.; Lee, C. L.; Choi, W. K. Emissive ZnO−Graphene Quantum Dots for White-Light-Emitting Diodes. *Nat. Nanotechnol.* **2012**, *7*, 465−471.

(21) Peng, J.; Gao, W.; Gupta, B. K.; Liu, Z.; Romero-Aburto, R.; Ge, L.; Song, L.; Alemany, L. B.; Zhan, X.; Gao, G.; Vithayathil, S. A.; Kaipparettu, B. A.; Marti, A. A.; Hayashi, T.; Zhu, J. J.; Ajayan, P. M. Graphene Quantum Dots Derived from Carbon Fibers. *Nano Lett.* **2012**, *12*, 844−849.

(22) Nurunnabi, M.; Khatun, Z.; Reeck, G. R.; Lee, D. Y.; Lee, Y. Near Infrared Photoluminescent Graphene Nanoparticles Greatly Expand their use in Noninvasive Biomedical Imaging. *Chem. Commun.* **2013**, *49*, 5079−5081.

(23) Nurunnabi, M.; Khatun, Z.; Huh, K. M.; Park, S. Y.; Lee, D. Y.; Cho, K. J.; Lee, Y. *In Vivo* Biodistribution and Toxicology of Carboxylated Graphene Quantum Dots. *ACS Nano* **2013**, *7*, 6858−6867.

(24) Maune, B. M.; Borselli, M. G.; Huang, B.; Ladd, T. D.; Deelman, P. W.; Holabird, K. S.; Kiselev, A. A.; Alvarado-Rodriguez, I.; Ross, R. S.; Schmitz, A. E.; Sokolich, M.; Watson, C. A.; Gyure, M. F.; Hunter, A. T. Coherent Singlet-Triplet Oscillations in A Silicon-Based Double Quantum Dot. *Nature* **2012**, *481*, 344−347.
(25) Petta, J. R.; Johnson, A. C.; Taylor, J. M.; Laird, E. A.; Yacoby, A.; Lukin, M. D.; Marcus, C. M.; Hanson, M. P.; Gossard, A. C. Coherent Manipulation of Coupled Electron Spins in Semiconductor Quantum Dots. *Science* **2005**, *309*, 2180−2184.
(26) Bluhm, H.; Foletti, S.; Neder, I.; Rudner, I.; Mahalu, D.; Umansky, V.; Yacoby, A. Dephasing Time of Gaas Electron-Spin Qubits Coupled to A Nuclear Bath Exceeding 200 ms. *Nat. Phys.* **2011**, *7*, 109−113.
(27) Bonaccorso, F.; Sun, Z.; Hasan, T.; Ferrari, A. C. Graphene Photonics and Optoelectronics. *Nat. Photonics* **2010**, *4*, 611−622.
(28) Li, L.; Nurunnabi, M.; Nafiujjaman, M.; Lee, Y.; Huh, K. M. A Photosensitizer-Conjugated Magnetic Iron Oxide/Gold Hybrid Nanoparticle as an Activatable Platform for Photodynamic Cancer Therapy. *J. Mater. Chem. B* **2014**, *2*, 2929−2937.
(29) Khatun, Z.; Nurunnabi, M.; Cho, K. J.; Byun, Y.; Bae, Y. H.; Lee, Y. Oral Absorption Mechanism and Anti-Angiogenesis Effect of Taurocholic Acid-Linked Heparin-Docetaxel Conjugates. *J. Controlled Release* **2014**, *177*, 64−73.
(30) Nurunnabi, M.; Khatun, Z.; Nafiujjaman, M.; Lee, D. G.; Lee, Y. Surface Coating of Graphene Quantum Dots using Mussel Inspired Polydopamine for Biomedical Optical Imaging. *ACS Appl. Mater. Interfaces* **2013**, *5*, 8246−8253.
(31) Obaid, G.; Chambrier, I.; J, M. Cook; Russell, D. A. Targeting the Oncofetal Thomsen−Friedenreich Disaccharide Using Jacalin-Peg Phthalocyanine Gold Nanoparticles for Photodynamic Cancer Therapy. *Angew. Chem., Int. Ed.* **2012**, *51*, 6158−6162.
(32) Yang, K.; Zhang, S.; Zhang, G.; Sun, X.; Lee, S. T.; Liu, Z. Graphene in Mice: Ultrahigh *in Vivo* Tumor Uptake and Efficient Photothermal Therapy. *Nano Lett.* **2010**, *10*, 3318−3323.
(33) Li, M.; Yang, X.; Ren, J.; Qu, K.; Qu, X. Using Graphene Oxide High Near-Infrared Absorbance for Photothermal Treatment of Alzheimer's Disease. *Adv. Mater.* **2012**, *24*, 1722−1728.
(34) Liu, Y.; Wang, G.; Huang, Q.; Guo, L.; Chen, X. Structural and Electronic Properties of T Graphene: a Two-Dimensional Carbon Allotrope with Tetrarings. *Phys. Rev. Lett.* **2012**, *108*, 225505−225509.
(35) Nurunnabi, M.; Cho, K. J.; Choi, J. S.; Huh, K. M.; Lee, Y. Targeted Near-IR Qds-Loaded Micelles for Cancer Therapy and Imaging. *Biomaterials* **2010**, *31*, 5436−5444.